Design and Extensive NPR Characterization of a Highly Linear SatCom GaN MMIC Doherty PA

Design and Extensive NPR Characterization of a Highly-Linear SatCom GaN MMIC Doherty PA

Anna Piacibello, *Member, IEEE,* Ricardo Figueiredo, *Member, IEEE,* Roberto Quaglia, *Member, IEEE,* Rocco Giofrè, *Senior Member, IEEE,* Paolo Colantonio, *Fellow, IEEE,* Nuno Borges Carvalho, *Fellow, IEEE,* Vittorio Camarchia, *Senior Member, IEEE*

***Abstract*—This paper presents the design strategy and extensive Noise-to-Power Ratio (NPR)-focused characterization of a state-of-the-art Doherty Power Amplifier for satellite applications in the Ka-band downlink (17.3–20.3 GHz), fabricated using a commercial 100-nm GaN-Si High Electron Mobility Transistor technology. The design aims for high gain and good intrinsic linearity over a 3 GHz bandwidth by adopting an amplifying chain with limited phase distortion and a Doherty combiner designed to compensate this residual phase distortion, and by optimizing the baseband impedance. Single-tone experimental characterization of the fabricated chip shows that it maintains an output power of 36 dBm with a power-added efficiency of 30% across the entire band. The linearity characterization explores the effects of signal statistics and nonlinear dynamics on NPR and discusses critical aspects concerning the comparability of different measurements. Modulations with instantaneous bandwidths up to a record of 2.9 GHz are explored, under which the Doherty PA is able to maintain PAE of at least 25% at 15 dB NPR. This demonstrates the amplifier's excellent linearity, achieving state-of-the-art performance among integrated power amplifiers for satellite communications.**

***Index Terms*—Doherty power amplifier, GaN, Linearity, MMIC, NPR, Satellite.**

I. Introduction

THE ongoing shift towards higher carrier frequencies, multi-carrier signals, and complex modulations with large Peak-to-Average Power Ratio (PAPR) [1], [2], such as Quadrature Amplitude Modulation (QAM) and Orthogonal Frequency-Division Multiplexing (OFDM), significantly impacts the design of power amplifiers (PAs), influencing both energy consumption and linearity. The effort to increase energy efficiency is crucial in satellite transmitters, as it affects power budgets, thermal design, overall weight, and ultimately cost [3]–[5].

The Doherty power amplifier (DPA) [6], [7] sets the standard for efficiency at cellular frequencies. However, extending its use to the Ka-band for satellite transmissions poses challenges due to high power requirements, effective thermal management, and the need for superior linearity across wide bandwidths. Current literature demonstrates promising results in power, gain, and efficiency but often lacks sufficient intrinsic linearity, necessitating additional linearizers [8], [9]. Reducing the use of linearizers is desirable to reduce cost, weight, and complexity, making the development of highly linear PAs crucial, especially for wide instantaneous bandwidths.

The linearity metric of reference for the system level characterization is the Noise-to-Power Ratio (NPR). The necessity of accurately measuring NPR in the context of Satellite Communications (SatCom) systems is well established [10]. However, the absence of a standardized NPR measurement methodology [11], coupled with insufficient details in existing characterizations, complicates the critical task of comparing linearity performance among DPAs designed for satellite applications. Many studies in the field present NPR results without explicitly specifying all crucial test conditions such as signal statistics, instantaneous bandwidth of the test signals, and the waveform characteristics of the baseband signal [8], [12]–[15]. This lack of specificity undermines the ability to confidently define and achieve target NPR performance levels, as these results are significantly influenced by the test conditions themselves [16].

Extensive literature highlights the impact of nonlinear dynamics and signal statistics on NPR and overall linearity [11], [16], [17], underscoring the imperative of incorporating these factors into the design, measurement, and reporting of PA system-level linearity. Understanding and properly accounting for these influences are essential steps towards ensuring accurate and meaningful assessments of DPA performance in wideband SatCom applications.

The design presented in this paper focuses on achieving intrinsic high linearity in a three-stage Monolithic Microwave Integrated Circuit (MMIC) GaN-Si DPA for the satellite downlink Ka band (17.3–20.3 GHz). This is achieved by minimizing the amplitude-to-phase modulation (AM/PM) distortion, a known problem of DPAs in single-tone operation [18]–[21], and by optimizing the baseband termination of the transistors to minimize its impact on the third-order Inter-Modulation Ratio (IMR) in two-tone operation. Furthermore, a balanced architecture is employed to further minimise third-order IMR [22], [23].

The paper expands on the content presented at the 2024 International Microwave Symposium (IMS) [24], which included the small and large signal single-tone continuous wave (CW) characterization of the DPA, by providing insights on the design techniques used to improve linearity and presenting an extensive linearity characterization.

Manuscript received Month Dd, Year; revised Month Dd, Year. (*Corresponding author: Anna Piacibello*)

A. Piacibello and V. Camarchia are with the Politecnico di Torino, 10129 Turin, Italy. e-mail: anna.piacibello@polito.it

R. Figueiredo and N.B. Carvalho are with the Instituto de Telecomunicações, 3810-193 Aveiro, Portugal.

R. Quaglia is with Cardiff University, Cardiff CF24 3AA, Wales, UK.

R. Giofrè and P. Colantonio are with the University of Roma Tor Vergata, 00133 Rome, Italy.

The adopted design strategy is based on the optimization of linearity in single- and two-tone conditions. The characterization aims at highlighting that, despite system-level linearity under modulated signal excitation differs from linearity in single- and two-tone operation, the adopted design strategy provides a successful method to design a DPA that also features state-of-the-art linearity at system level.

To the best of our knowledge, the paper presents the most extensive NPR characterization of DPAs reported to date, achieving an unprecedented instantaneous bandwidth of 2.9 GHz. The DPA performance under this wideband excitation represents state-of-the-art advancements in both NPR assessment and DPA design. Additionally, this characterization work elucidates how linearity performance can be better compared between state-of-the-art designs. The comprehensive characterization campaign investigates the influence of amplitude statistics and instantaneous bandwidth on NPR, highlights the limitations of estimating NPR from two-tone measurements, and emphasizes the importance of precisely defining all relevant parameters when establishing target NPR performance. The goal is to help clearly establish the test conditions necessary to ensures an accurate assessment of the true linearity performance of wideband amplifiers, providing valuable insights for future design and optimization in SatCom systems.

The manuscript is organized as follows. Section II describes the design strategy, focusing on the aspects that are related to linearity and its optimization. Section III presents the large signal CW characterization of the DPA, summarizing the single-tone results presented in detail in [24] and including the two-tone results. The extensive NPR characterization is presented in Section IV, which explores the influence of signal statistics and nonlinear dynamics on NPR, discusses the comparison of two-tone and system level linearity, and provides indications for an unambiguous definition of the target NPR performance. Finally, conclusions are drawn in Section V.

II. Design strategy

A. Specifications

The aim of this design is to cover the satellite Ka-band downlink (17.3–20.3 GHz) with a single-chip GaN DPA able to provide 36 dBm of output power while maintaining a Power-Added Efficiency (PAE) around 35% and a high intrinsic linearity. The linearity target is expressed in terms of NPR, which should be higher than 15 dB in all conditions. Since the NPR is typically difficult to predict at simulation level during the design, the linearity specification is translated for design purposes to AM/PM, which should be maintained within $\pm 15^\circ$ [8]. Furthermore, the small signal gain should be of the order of 30 dB, and input and output return losses higher than 15 dB. All specifications should be guaranteed while maintaining the transistors' maximum junction temperature (T_j) below 160 °C in all conditions.

B. Architecture definition

The adopted technology is the 100-nm gate length GaN-Si HEMT process by OMMIC, which features around 2.25 W/mm at 9-V drain supply voltage, already accounting for the required space derating. This allows maintaining the maximum T_j below the specified threshold, but forces to combine several transistors in the final stage to comply with the output power specification. Given the need to design based on a reliable large signal model to predict the power- and frequency-dependent signal de-phasing that typically occurs in DPAs, the choice is to combine four 8×100 µm devices, for which the foundry provides a non-linear and thermal model. Accounting for the gain penalty typical of the DPAs and a gain around 10 dB for the individual transistor, two stages are needed to drive the power devices. For an optimum trade-off of efficiency and linearity, drivers with peripheries of 6×50 µm and 2×50 µm are inserted in each of the DPA branches, leading to a fully symmetric structure.

Among several on-chip power combination strategies, detailed and preliminarily explored in [25], it was chosen to implement two individual DPA cells with half of the target power rating adopting a single 8×100 µm device in each branch, and to operate them in a balanced configuration by means of input and output Lange couplers, as shown in the block diagram of Fig. 1. This has the twofold advantage of providing excellent input and output return losses and to ease the output matching over a wide band. The latter is due to a reduced impedance transformation compared to the case where two devices are combined in parallel in each of the DPA branches, which halves the optimum load impedance. Another advantage of the balanced architecture is related to the partial cancellation of high order terms and its beneficial impact on the linearity. In fact, while the AM/PM of the single DPA cell and of the balanced one is the same, the odd IMRs, in particular the third-order one, result lower in the balanced structure thanks to the cancellation induced by the quadrature couplers [23]. On the other side, combined and balanced MMIC DPAs have a complex routing of the bias lines and result in somewhat larger areas. Further details on the choice of the bias points for the various devices are provided in [24].

Fig. 2 shows the microscope picture of the MMIC (a), whose dimensions are 5×6 mm^2, and the assembled test jig (b). The top DPA cell is highlighted by a red box, and the layout follows the scheme of Fig. 1, with the Main branches on the internal part of the chip and the Auxiliary branches close to the border for an easier routing of the bias lines.

C. AM/PM Minimization

As a key feature of this state-of-the-art DPA design, a flat AM/PM characteristic has been obtained from the combination of a relatively linear three-stage amplifier chain and a Doherty combiner which limited the phase distortion of the output section. With reference to the scheme of principle of Fig. 1, the overall AM/PM of the DPA is estimated as

$$\mathrm{AM/PM_{DPA}}(V_\mathrm{s}) = \angle\frac{V_\mathrm{out,DPA}}{V_\mathrm{in,DPA}}(V_\mathrm{s}) - \angle\frac{V_\mathrm{out,DPA}}{V_\mathrm{in,DPA}}\bigg|_\mathrm{ss}, \quad (1)$$

where the subscript "ss" indicates the small signal condition, which serves as normalization for the phase variation dependent on the source voltage V_s. It is found that the overall AM/PM is given by the contribution of two effects, namely of

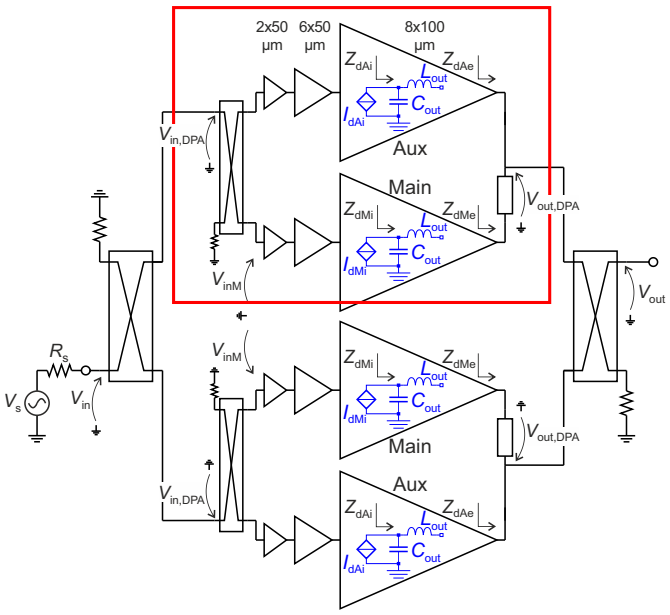

Fig. 1. Block diagram of the architecture of the fabricated MMIC DPA.

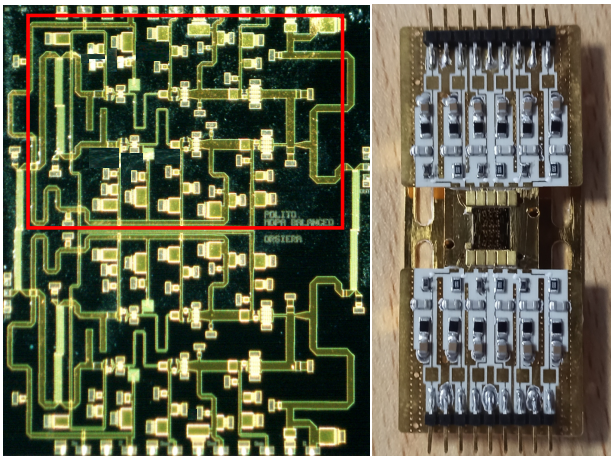

(a) (b)

Fig. 2. Microscope photograph of the fabricated GaN-Si MMIC DPA (a), with the DPA cell enclosed by a red box, and assembly in test jig with dc decoupling (b). The chip size is $5\times6\text{mm}^2$.

the amplifying chain and of the output section. The latter is the phase variation of the output voltage normalized to that of the Main drain current and is induced by the current injected by the Auxiliary. They can be isolated as follows:

$$\angle\frac{V_{\text{out,DPA}}}{V_{\text{in,DPA}}} \approx \angle\frac{V_{\text{out,DPA}}}{V_{\text{inM}}} = \angle\left(\frac{V_{\text{out}}}{I_{\text{dMi}}}\cdot\frac{I_{\text{dMi}}}{V_{\text{inM}}}\right) = \angle\left(\frac{V_{\text{out}}}{I_{\text{dMi}}}\right)\Big|_{\text{out}} + \angle\left(\frac{I_{\text{dMi}}}{V_{\text{inM}}}\right)\Big|_{\text{amp}}, \quad (2)$$

which relies on the approximation that the main contribution to phase distortion in a DPA comes from the Main branch [19] and amounts to $\text{AM/PM}_{\text{DPA}} \approx \text{AM/PM}_{\text{out}} + \text{AM/PM}_{\text{amp}}$.

The AM/PM of the amplifier chain has been simulated using the foundry large signal model and it is reported in Fig. 3. The AM/PM of the output section has been firstly estimated

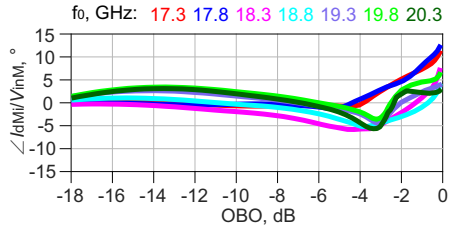

Fig. 3. AM/PM profile of the three-stage amplifying chain from 17.3 GHz to 20.3 GHz, estimated adopting the nonlinear foundry transistor nonlinear model.

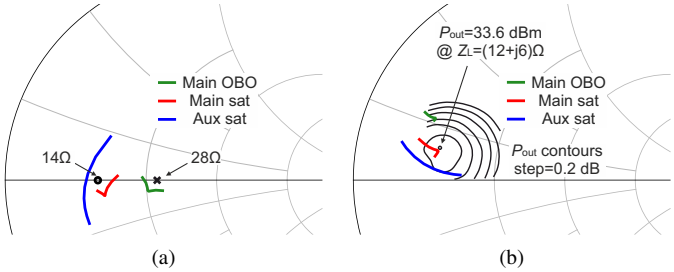

(a) (b)

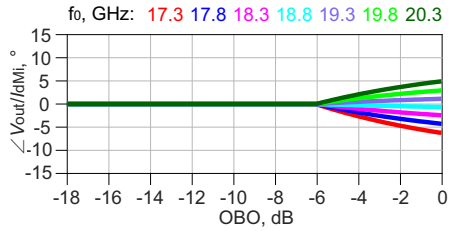

(c)

Fig. 4. Simulation of the output section from 17.3 GHz to 20.3 GHz adopting the linear model for the Main and Aux final-stage devices: synthesized loads at the (a) current generator and (b) extrinsic planes, and (c) AM/PM profile.

adopting a linear simulation setup, where the transistors are represented as ideal current sources loaded by a linear LC equivalent of their output parasitic elements as shown in blue in Fig. 1. This setup has been used to optimize the combiner so as to provide the desired matching condition to the Main and Auxiliary stages as well as synthesizing an AM/PM profile that compensates the phase distortion of the amplifying chain. In particular, the combiner has a topology analogous to the one in [9] and aims to synthesize a slight phase compression when the amplifying chain has a phase expansion, and vice versa. The optimum load of the devices has been first estimated at the current generator planes (Z_{dMi}, Z_{dAi} indicated in Fig. 1) according to load line considerations, which lead to $R_{\text{opt}} = 14\,\Omega$, and then confirmed by a load pull measurement campaign on bare die devices [26], which predicted an optimum impedance of $(12 + j6)\,\Omega$ at the extrinsic drain plane (Z_{dMe}, Z_{dAe} in Fig. 1) and resulted in line with the initial estimation. The simulated loads and AM/PM synthesized by the output section are reported in Fig. 4 in the range 17.3–20.3 GHz. A good output matching is maintained over the whole bandwidth while also synthesizing a phase characteristic that can compensate quite well that of the amplifying chain. The compensation is almost exact around 17.3 GHz, whereas at 20.3 GHz the chain has almost

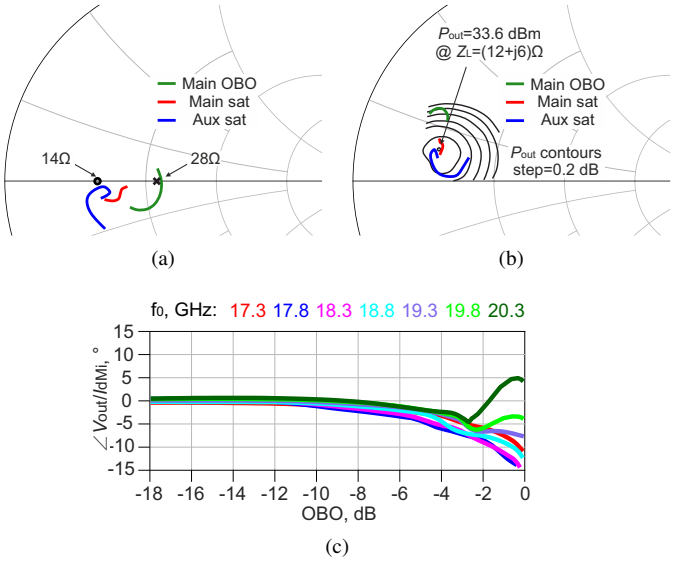

Fig. 5. Simulation of the output section from 17.3 GHz to 20.3 GHz adopting the full non-linear models of the active devices and electromagnetic models of all passive structures: synthesized loads at the (a) current generator and (b) extrinsic planes, and (c) AM/PM profile.

null distortion and the combiner has a slight expansion, thus leading to an overall AM/PM that is slightly positive.

Additionally, the linear simulation has proved to provide a very good approximation of the actual nonlinear simulation adopting the full foundry model, which is reported in Fig. 5. In fact, both the synthesized loads and the phase distortion profile follow quite closely the predicted trend, the main difference being a slightly late turn-on the Auxiliary branch in the complete DPA compared to the case where the output section is simulated standalone.

D. Optimization of the Baseband Termination

As a more accurate indicator of the linearity of the DPA that also accounts for memory effects, a two-tone test with variable spacing is performed during the design phase to evaluate and optimize the linearity of the DPA and the impact of its memory effects, especially as the Instantaneous Bandwidth (IBW) required by the target application increases. This can also aid the optimization of the baseband impedance presented by the matching networks to the gate and drain terminals of the transistors.

Research has reported that the intermodulation of an FET amplifier is also affected by the impedance presented to the device at baseband frequencies, i.e., those of the modulating signal or, in a multi-carrier system, the difference frequencies [27]. The baseband impedance is usually dominated by the bias network. The detrimental effects come from a variation of instantaneous baseband voltage, which decreases the available RF voltage swing on the drain of the devices, leading to earlier clipping and distortion compared to the cases where the voltage variations were reduced thanks to lower baseband impedance [28]. It has been demonstrated in [29] that the device's drain baseband impedance has the dominant effect on intermodulation. There is a trade-off between minimizing the intermodulation distortion and its independence from baseband impedance, which is determined by the device's gate bias voltage. The work in [30] shows that optimum values for baseband impedance can be found experimentally and compensate for harmonic effects. The input impedance observed by the gate starts showing an impact only if the drain impedance can be optimized [31]. However, realistically targeting optimum values would require a very accurate knowledge of the nonlinear mechanisms. Therefore, as the drain impedance at the second harmonic frequencies is strongly reactive, a more practical approach is to minimize the baseband impedance to reduce IMD asymmetry [27].

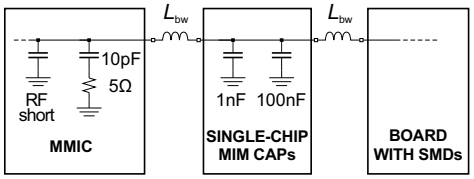

Fig. 6. Schematic of the decoupling network included on all the DC lines.

The selection of the elements in the bias network, both on and off chip, is a result of a delicate trade-off between controlling the baseband impedance, ensuring stability, and making the in-band operation insensitive to the off-chip components. As final arrangement, one level of DC decoupling on the bias lines is included on chip, namely 10 pF capacitor with a small resistor in series to dampen the resonance with the inductance of the backvia. After the DC pads, the MMIC is wire bonded to an external DC decoupling board including two additional levels of capacitors of the order of 1 nF and 100 nF (see Fig. 6). The bondwire inductance L_{bw} is estimated to be approximately 0.2–0.4 nH, depending on the length required to reach the corresponding off-chip pad as well as the number of wires. The value of the capacitors and of the series resistors is tuned in such a way to avoid sharp resonances leading to high baseband impedance values. The external board can be customized to have extra levels of surface-mount shunt capacitors and includes 0 Ω series resistors which can be replaced with other values based on the need. In this case, the default values for the shunt capacitors are 1 nF and 100 nF. The resulting impedance at the drain of the transistors in the final stage is shown in Fig. 7 for variable bondwire inductance in the identified range of values. As per the original project specifications, the baseband impedance has been optimized primarily for IBW of the order of 100 MHz and foreseeing operation with signal bandwidths which could reach 1 GHz. The range of interest for this analysis is therefore considered to be from 1 MHz to 3 GHz, which coincides with the full RF bandwidth of the DPA and constitutes the limit for the IBW that can be adopted for the modulating signal. It can be seen that the magnitude of the baseband impedance is rather constant and nearly null up to 100 MHz, and then increases until reaching about 40–50 Ω at 3 GHz. Around 1 GHz, it becomes comparable with the optimum load of the transistor ($\approx$ 20 Ω). The value of the bondwire inductance slightly affects the monotonicity of the curve but has no significant impact on the magnitude value.

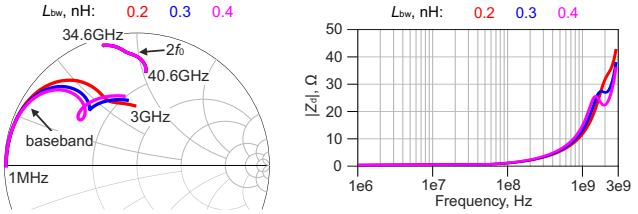

(a) (b)

Fig. 7. Impedance synthesized at the drain of the of the transistors in the final stage, for bondwire inductance values 0.2–0.4 nH: (a) on the Smith chart normalized to 50 Ω, and (b) magnitude at baseband frequencies.

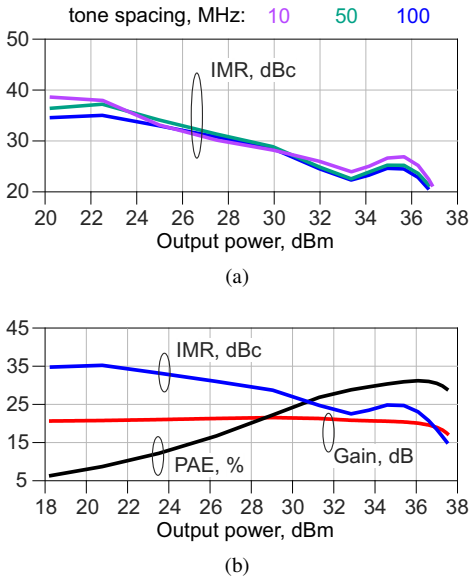

(a)

(b)

Fig. 8. Simulated performance versus output power under two-tone excitation around 18.8 GHz: (a) IMR for different tone spacings and (b) gain, PAE and IMR for 100 MHz tone spacing.

Fig. 8(a) reports the simulated IMR under two-tone operation around 18.8 GHz with variable tone spacing, assuming $L_{\rm bw} = 0.4$ nH. The estimated performance with 100-MHz tone spacing is shown in Fig. 8(b). The ability of the DPA to maintain a high level of linearity up to near saturation, in agreement with the prediction of the AM/PM and also thanks to the presence of a sweet spot around 34–36 dBm, is confirmed by this test.

III. CW Characterization

Fig. 9 summarizes the achieved CW performance by comparing the simulated and measured power sweeps in the frequency band 17.3 GHz–20.3 GHz.

The DPA maintains the required saturated output power of 36 dBm and a PAE higher than 23% in the whole 6 dB OBO region, while showing a limited gain compression and an AM/PM within ±12° over the whole the full 17.3–20.3 GHz band. Notably, the measured performance closely matches simulation predictions regarding gain level and compression, efficiency, and AM/PM maximum values, thus demonstrating some good accuracy of the nonlinear model of the transistors, which is an essential element for a successful DPA design.

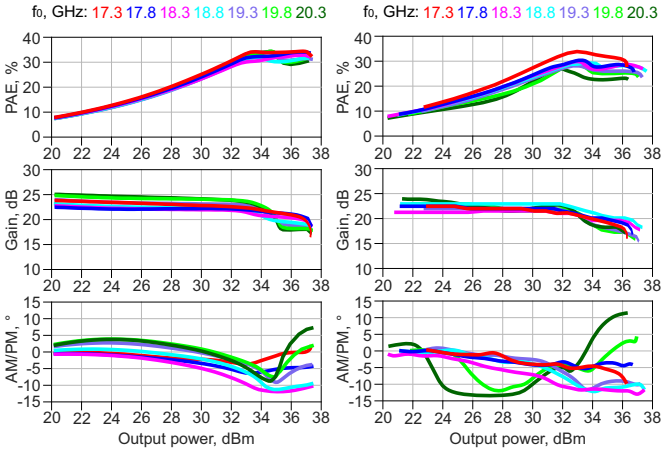

(a) (b)

Fig. 9. Comparison of (a) simulated and (b) measured CW performance from 17.3 GHz to 20.3 GHz.

Table I reports the comparison with the state of the art of the CW performance of MMIC DPAs at similar frequencies.

TABLE I
CW Performance of state-of-the-art GaN DPAs for Ka-band satellite applications.

Sub.	Freq. (GHz)	$P_{out,sat}$ (dBm)	PAE_{sat} (%)	PAE_{6dB} (%)	G_{sat} (dB)	Ref.
SiC	20	35	37	18*	17*	[13]
SiC	17.3-20.3	41.5	35	28	20	[8]
Si	16.3–20.3	36.6	21	19	18	[9]
Si	17.3-20	36.3	24	18	20	[32]
Si	**17.3–20.3**	**36**	**23**	**23**	**15**	**T.W.**

* Value extrapolated from graphs

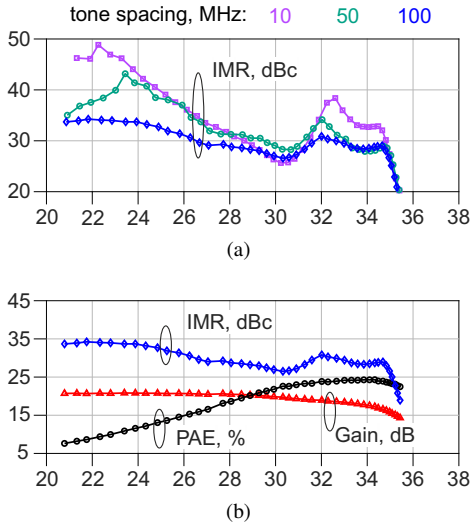

(a)

(b)

Fig. 10. Measured performance versus output power under two-tone excitation around 18.8 GHz: (a) IMR for different tone spacings and (b) gain, PAE and IMR for 100 MHz tone spacing.

Additionally, a two-tone characterization has been performed at the centre frequency of 18.8 GHz to provide insights on the link with the design strategy and the performance expected from simulations. The results are reported in Fig. 10.

Apart from a slightly lower PAE, which is also in line with the results of the single-tone characterization, the measured performance is in good agreement with the simulations of Fig. 8. In particular, the IMR level in the linear region is quite well captured, especially in the 100-MHz spacing case, as is the position and the extension of the sweet spot.

IV. System Level Linearity Characterization

While AM/PM and IMR metrics are convenient for aiding PA design [33], they have limitations. Gain compression and phase shift provide limited insight into co-channel distortion under modulated signal operation, and IMR does not fully capture adjacent channel distortion. CW and two-tone signals do not cover the full instantaneous bandwidth of modulated signals, meaning they do not excite all relevant nonlinear dynamics [11]. In some systems, signal statistics change over time by dynamically adjusting modulation, thus requiring optimal operation across different PAPRs. Despite these limitations, CW and two-tone signals are used for PA design due to the lack of guidance for real communication signals. Preliminary work [34] suggests that wideband active load-pull systems could help develop wideband design strategies following a measurement-based approach, but EDA approaches are still missing. Challenges in modulated signal-based design are long simulation times and inaccurate wideband models that might mislead design choices. However, system-level linearity under modulated signal operation differs from linearity in CW or two-tone operation. This section aims to highlight these differences while showcasing that, despite the inherent limitations, our design approach leads to good linearity performance. For that, we focus on NPR, the key system level figure of merit for linearity in SatCom [10].

NPR measures the ratio of co-channel uncorrelated distortion power spectral density to the signal power spectral density at the system output [11]. We use the notch technique to measure NPR, employing a band-limited white noise multi-tone with a central notch as the input signal [35]. The baseband multi-tone signal is designed to ensure the desired amplitude statistics in each test scenario [36]. Critical design parameters of an equally spaced, equal magnitude multi-tone signal include the phase distribution, which determines the amplitude statistics; the instantaneous bandwidth occupied by the signal; the number of tones, which, in conjunction with the bandwidth, sets the carrier spacing frequency and the resolution frequency of the multi-tone (i.e., the slowest memory observable); and the number of switched-off tones, which directly defines the notch bandwidth as a percentage of the total instantaneous bandwidth.

Our experimental setup, depicted in Fig. 11, includes a Keysight M8190A Arbitrary Waveform Generator (AWG) for generating the baseband signal, a Keysight E8267D Vector Signal Generator (VSG) for up-conversion, and a Keysight N9041B Vector Signal Analyzer (VSA) for down-conversion and waveform capture. Pre-drivers and a directional attenuator are used to ensure proper signal amplification and accurate measurement. For each NPR measurement, the average input power is varied in small steps from small signal up to saturation, and NPR is evaluated at the DPA output by comparing

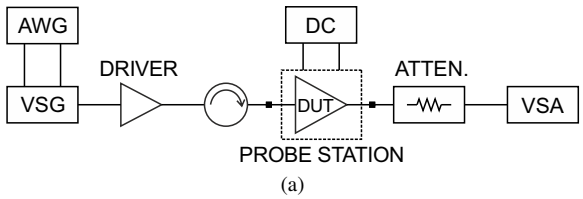

(a)

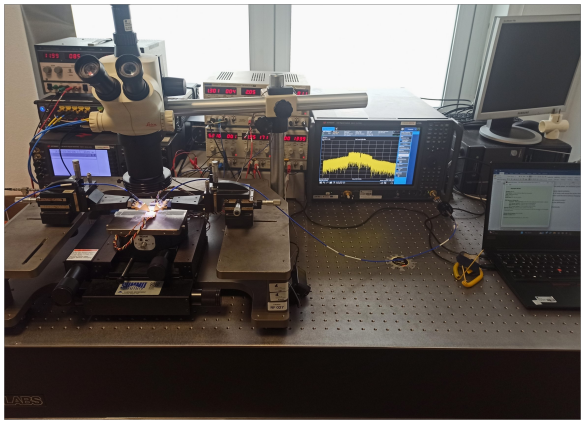

(b)

Fig. 11. Experimental setup for the NPR characterization.

the average power spectral density of the deactivated tones to the one of the activated tones.

The following sections present a characterization campaign devised to demonstrate the influence of amplitude statistics and instantaneous bandwidth on NPR, highlight the limitations of estimating NPR from two-tone measurements, and emphasize the need to clearly define all relevant parameters when setting a target NPR performance for a design.

A. Influence of Signal Statistics on NPR

To investigate how signal amplitude statistics affects NPR, we used two band-limited white noise signals realized with multi-tones, both having an instantaneous bandwidth of 100 MHz but different amplitude distributions. One signal has a Gaussian amplitude distribution, as used in the formal NPR definition [37], and approximately 10 dB PAPR. The other signal has a uniform amplitude distribution with approximately 3 dB PAPR, resembling the PAPR characteristics of the target application.

The multi-tone parameters for each distribution differ slightly, as detailed in Table II. This approach ensures that observed changes are attributable to differences in amplitude statistics, while the excitation of nonlinear dynamics remains constant.

TABLE II
100 MHz Multi-Tone Design Parameters

Statistics	Tones	Resolution	Notch Tones	Notch % BW
Gaussian	10001	10 kHz	401	4 %
Uniform	2001	50 kHz	201	10 %

Experimental results are presented for three carrier frequencies in the band of interest: 17.3 GHz, 18.8 GHz, and

20.3 GHz. Fig. 12 and 13 show the results for the Gaussian and uniform signals, respectively.

For the Gaussian signal, an NPR sweet spot was observed around 32 dBm of average output power, corresponding to 4 dB OBO relative to the saturated output power identified during CW characterization. This point coincides with the best PAE, maintaining at least 20 dB NPR at this operational point for all frequencies of interest. At 34 dBm (2 dB OBO, approximately 8 dB clipping for the 10 dB PAPR signal), the NPR exceeds 15 dB, and the PAE is similar to that at 4 dB OBO.

The uniform signal results demonstrate excellent linearity, maintaining NPR higher than 15 dB in all conditions, even under significant clipping, where the average output power of the modulated signal approaches the maximum power achieved in the CW measurement. Up to 1 dB from the saturation power of 36 dBm, the NPR remains above 20 dB, with corresponding PAE above 20% at all tested frequencies.

Comparing CW, Gaussian, and uniform signal results reveals the influence of statistics on NPR. The uniform signal results are more similar to CW results than the Gaussian signals. The uniform signals can achieve 1 dB OBO power, whereas Gaussian signals reach only 2 dB OBO. The efficiency and gain curves for uniform signals are more aligned with CW than Gaussian signals. Notably, at 20.3 GHz, the uniform gain trend matches CW, while the Gaussian gain does not. Although Gaussian signals reach peak PAE similar to CW, it is only within a narrow power range (31-33 dBm). In contrast, uniform signals maintain peak efficiency over a broader range (31–36 dBm), similar to CW.

Linearity is significantly worse with Gaussian signals. At the same average power, the peak power of Gaussian signals force the DPA into deeper compression states than uniform signals [16]. Fig. 14 illustrates that ignoring the influence of signal statistics on device linearity can be catastrophic. It shows similar average output power levels and roughly similar gain and efficiency trends but more than a tenfold difference in linearity. A small degradation of about 1.5 dB in the power gain was observed for the same bias conditions from the first (uniform) to the second (Gaussian) NPR measurement campaign, attributed mainly to the wear-out of the RF probe contacts, as well as to the extensive power sweeps that have been performed throughout the full characterization of the same chip, which extended up to significant compression. This also demonstrates the robustness of the technology and of the design.

This study highlights the known effects of signal statistics on system linearity [16], as observed in NPR, the critical linearity performance indicator in SatCom. Therefore, these factors must be considered when defining linearity performance goals.

B. Influence of Nonlinear Dynamics on NPR

The impact of nonlinear dynamics on PA linearity is well-established [17]. Recent studies using NPR-like measurements show how these dynamics manifest under modulated signal conditions [11]. This section provides empirical evidence of nonlinear dynamics' influence on DPA linearity through NPR analysis at different carrier frequencies or with varying instantaneous bandwidths at the same carrier frequency. To isolate the influence of nonlinear dynamics, in this case we fixed all signal parameters except for carrier frequency and instantaneous bandwidth.

By revisiting the 100 MHz bandwidth NPR measurements presented earlier, we can observe the impact of nonlinear dynamics across different carrier frequencies for the same signal statistics. For the Gaussian distribution, shown in Fig. 12, the NPR trend is similar across different carrier frequencies. The influence of nonlinear dynamics is subtle, as this distribution does not evenly excite both small and large signal dynamics [16], [38]. However, careful examination reveals differences. At 17.3 GHz and 18.8 GHz, the gain characteristic is very similar. At 32 dBm, the NPR sweet spot is nearly 25 dB, almost 5 dB higher at 18.8 GHz compared to 17.3 GHz. Correspondingly, the PAE at 17.3 GHz is approximately 32.5%, about 5% better than at 18.8 GHz, confirming the trade-off between linearity and efficiency. At 17.3 GHz and 20.3 GHz, the NPR characteristic with power is similar, with about 20 dB NPR at 32 dBm. Despite similar small signal gain, gain compresses much faster at 20.3 GHz, resulting in 25% PAE at that operating point, a 7.5% decrease compared to 17.3 GHz.

For the uniform distribution, shown in Fig. 13, the influence of nonlinear dynamics is more apparent, as the uniform distribution evenly excites small and large signal dynamics. Despite similar small signal gain trends, different NPR trends are observed. At 17.3 GHz, NPR monotonically decreases until the sweet spot. At 18.8 GHz, NPR remains constant between 22 dBm and 28 dBm. At 20.3 GHz, NPR exhibits two sweet spots, one at 27 dBm and another at 35 dBm. Similar trade-offs between gain compression, PAE, and NPR across frequencies are observed as in the Gaussian case.

These NPR differences are observed in measurements of the same DPA, with similar small signal behavior, excited with the same envelope signal, but operated at different carriers. This showcases the significant impact of nonlinear dynamic behavior on NPR. It highlights that the complexity extends beyond baseband treatment, as the same instantaneous bandwidth yields the same baseband impedance even when the carrier changes. Thus, nonlinear harmonic behavior plays a crucial role.

To further investigate the influence of nonlinear dynamics with varying instantaneous bandwidths, we conducted a study with fixed Gaussian statistics, as in the formal NPR definition, and a fixed carrier frequency of 18.8 GHz. We varied the instantaneous bandwidths: 100 MHz, 1 GHz, and 2.9 GHz (corresponding to the full DPA bandwidth). Signal characteristics are detailed in Table III. All signals have the same frequency resolution (10 kHz) and the same notch bandwidth percentage (4%). This approach guarantees that only the dynamics change, without skewing NPR measurement results.

Experimental results are displayed in Fig. 15. For measurements up to 1 GHz, the setup in Fig. 11 was used. For 2.9 GHz, instrumentation complexity increased significantly. The Keysight N9041B was operated as a VSA instead of an IQ receiver, with low resolution and video bandwidths (1 kHz) to

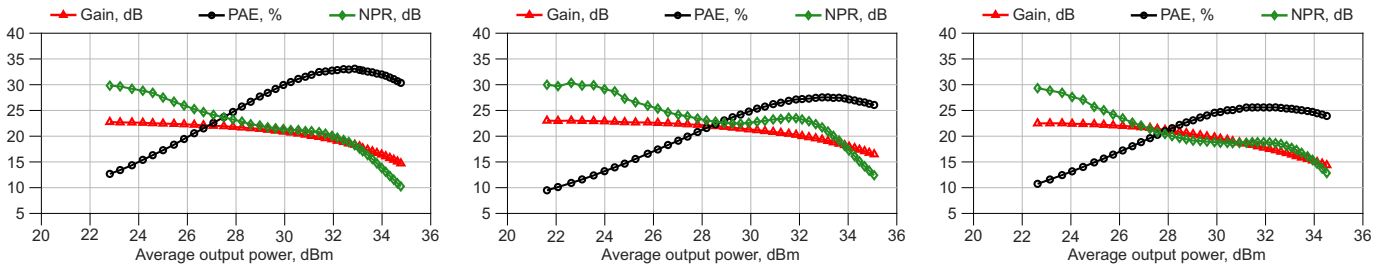

Fig. 12. Measured power gain, PAE and NPR versus average output power under 100-MHz Gaussian white noise excitation at different carrier frequency: (a) 17.3 GHz, (b) 18.8 GHz, (c) 20.3 GHz.

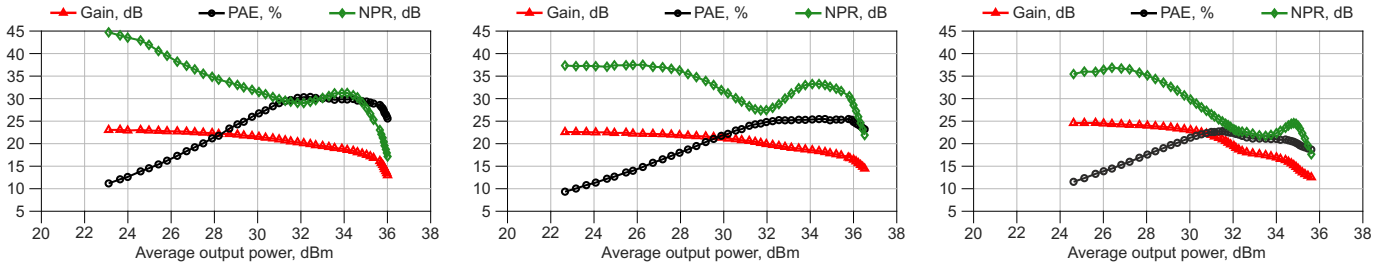

Fig. 13. Measured power gain, PAE and NPR versus average output power under 100-MHz uniform white noise excitation at different carrier frequency: (a) 17.3 GHz, (b) 18.8 GHz, (c) 20.3 GHz.

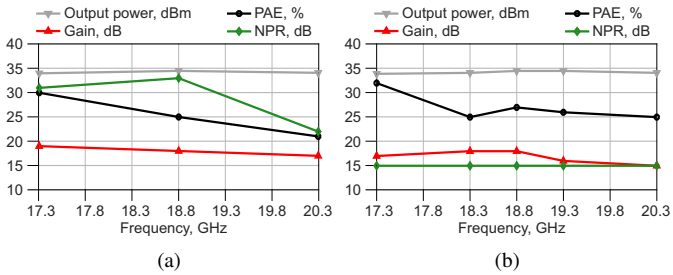

Fig. 14. Measured average performance (output power, power gain, PAE and NPR) versus carrier frequency under 100-MHz signal excitation with comparable average power: (a) uniform (3 dB PAPR) and (b) Gaussian (10 dB PAPR).

measure each tone clearly, and band stitching was necessary to meet the required resolution (10 MHz window, 10000 points). Nearly 300 measurements were needed for a single NPR point, with each measurement point taking about 30 minutes, plus 30 minutes for calibration. Due to these complexities, only the most relevant portion of the dynamic range, close to strong clipping where NPR falls below 15 dB, was captured for the 2.9 GHz measurement. These are state-of-the-art NPR measurements, the first of their kind to our knowledge using this method at such wide instantaneous bandwidths.

Results reveal similar gain and PAE trends with power for all bandwidths: at 30 dBm, PAE is approximately 25% for all bandwidths, and at 32 dBm, gain is roughly 20 dB, highlighting gain flatness and validating the design across all bandwidths. However, NPR trends indicate the presence of nonlinear dynamics. Comparing 100 MHz and 1 GHz measurements, the NPR sweet spot is absent at 1 GHz, and small signal values differ by a factor of 10 (around 30 dB for 100 MHz and 20 dB for 1 GHz). Different back-off levels are needed to meet 15 dB NPR: 2 dB OBO at 100 MHz, 4 dB OBO at 1 GHz, and 7 dB OBO at 2.9 GHz. As bandwidth increases, linearity degrades without a corresponding increase in PAE. For instance, comparing 100 MHz and 1 GHz at 32 dBm, NPR degrades by 10 dB (from 25 dB to 15 dB), while efficiency remains similar. Comparing 1 GHz and 2.9 GHz at 32 dBm, NPR degrades by 2 dB (from 15 dB to 13 dB), and PAE decreases by 2.5% (from 27.5% to 25%).

Experimental results demonstrate how bandwidth and carrier frequency influence NPR, highlighting the importance of accounting for nonlinear dynamic effects. Despite the current design strategy based on existing tools is not optimal for increasing instantaneous bandwidths, we were able to maintain cutting-edge performance even at bandwidths previously unexplored, achieving state-of-the-art DPA performance at record-breaking instantaneous bandwidths and validating the robustness of our design approach under challenging conditions. Future improvements could be achieved with advanced wideband design tools.

TABLE III
MULTI-TONE DESIGN PARAMETERS OF WHITE GAUSSIAN NOISE

Bandwidth	Tones	Resolution	Notch Tones	Notch % BW
100 MHz	10001	10 kHz	401	4 %
1000 MHz	100001	10 kHz	4001	4 %
2900 MHz	290001	10 kHz	11601	4 %

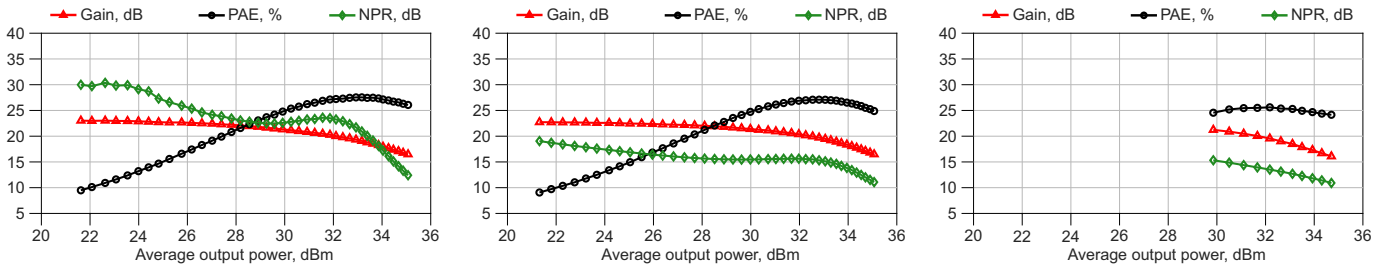

Fig. 15. Measured power gain, PAE and NPR versus average output power under Gaussian white noise excitation with 18.8 GHz carrier and IBW of: (a) 100 MHz, (b) 1 GHz, (c) 2.9 GHz.

C. NPR Measurement vs Two-Tone Approximation

NPR is frequently estimated based on two-tone IMR measurements, a method grounded in seminal work that established relationships between IMR and various linearity metrics [39]. For NPR, the relationship is given by:

$$\mathrm{NPR_{dB}} = \mathrm{IMR_{dB}} - 10 \cdot \log_{10}(6) = \mathrm{IMR_{dB}} - 7.7. \quad (3)$$

However, this approach has inherent limitations. The method is memoryless, considers only third-order nonlinearities, and implicitly assumes a Gaussian signal distribution. These constraints significantly limit its applicability in SatCom systems, which typically do not conform to these conditions. Specifically, two-tone signals are unable to excite the necessary bandwidth and have fixed statistics (6 dB PAPR [40]). Despite these limitations, the two-tone IMR method remains the only approach with sufficiently low complexity to be useful at the design stage.

To illustrate the limitations of this method, we compared NPR estimates from two-tone IMR measurements with actual NPR measurements using a Gaussian distribution at an 18.8 GHz carrier frequency and a 100 MHz bandwidth, as shown in Fig. 16. The analysis shows that while both methods predict the NPR sweet spot around 32 dBm and similar NPR values at saturation (approximately 12.5 dB at 35 dBm), IMR predictions fails to capture small signal dynamics and higher-order nonlinearities. This divergence becomes even more evident when comparing IMR with NPR measurements using different amplitude signal statistics, e.g., the uniform one of Fig 13.

Despite these discrepancies, the alignment between simulated and measured IMR results and their accurate identification of the NPR sweet spot and saturation NPR value for Gaussian statistics offer valuable insights. These findings can be leveraged using existing design strategies to achieve good DPA performance under wideband modulated signal conditions, as we have done in this work. It is essential, however, to start incorporating this broadband behavior into the design stage. The key takeaway is that while IMR-based NPR predictions provide useful information, designers must remain acutely aware of their limitations when inferring system-level linearity during the design process.

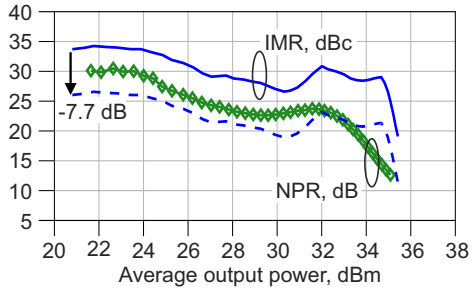

Fig. 16. Measured linearity performance versus output power in the multi-tone NPR test with 100-MHz IBW Gaussian noise (green, symbols) and two-tone test with 100 MHz tone spacing (blue, solid). The NPR estimation based on IMR given by (3) is also shown (blue, dashed).

TABLE IV
LINEARITY PERFORMANCE OF STATE-OF-THE-ART GAN DPAS FOR KA-BAND SATELLITE APPLICATIONS.

Modulation	f_0 (GHz)	IBW (GHz)	OBO (dB)	NPR* (dB)	PAE* (%)	Ref.
Gaussian	20	–	2.5+	15+	25+	[13]
DVB-32 APSK	18.7	1	4	15	27	[8]
SC-FDMA	18.7	1	6	20	26	
Gaussian	18.8	0.1	4	17.7	23	[9]
Uniform	**18.8**	**0.1**	**0**	**25**	**25**	**T.W.**
Gaussian	**18.8**	**0.1**	**1**	**15**	**27**	
Gaussian	**18.8**	**1**	**3**	**15**	**27**	
Gaussian	**18.8**	**2.9**	**6**	**15**	**25**	

* At the specified OBO + Simulated performance

D. How to Specify Target NPR Performance

Throughout the system-level linearity characterization analysis, we have placed significant emphasis on operation points achieving 15 dB or 20 dB NPR performance, a typical benchmark for linearity performance targets in SatCom. Our analysis has demonstrated that NPR performance is highly dependent on test conditions, specifically baseband signal statistics, carrier frequency, and instantaneous bandwidth. This dependency makes NPR performance challenging to compare across different tests, especially given the absence of a standardized NPR measurement methodology and only rough guidelines available in the literature [11], [16].

Table IV provides a comprehensive summary of NPR performance, comparing our results with those reported in state-of-the-art PA designs. This table details the NPR and corresponding power-added efficiency (PAE) at specified output back-off

(OBO) values, along with the conditions under which each test was performed. Our results show that the DPA exhibits excellent linearity with 100 MHz signals for both uniform and Gaussian statistical distributions, maintaining NPR above 15 dB almost up to saturation (0-1 dB OBO). The critical tests for verifying compliance with SatCom standards are those conducted with Gaussian signals with IBW greater than 1 GHz, where the DPA continues to display satisfactory linearity and non-degraded efficiency between 3 dB and 6 dB OBO.

Our findings demonstrate state-of-the-art performance, meeting the typical 15 dB NPR performance requirement at lower back-off levels, particularly for narrowband signals with uniform distribution. Remarkably, our DPA meets the criteria for 2.9 GHz instantaneous bandwidth, an unprecedented achievement. However, it is hard to have absolute confidence in performance comparisons in terms of NPR due to the different methods used for measurement in different state-of-the-art works.

To ensure comparable NPR results, it is essential to use multi-tone signals with the same distribution, frequency resolution, and notch bandwidth percentage, as utilized in this study. Standardized test waveforms can enhance confidence, repeatability, and comparability across different studies [16]. Correctly specifying NPR target performance for a power amplifier requires more than stating a metric value like 15 dB NPR. The target metric value must be defined within a specific context, including clearly defined signal statistics, carrier frequency, instantaneous bandwidth, minimum required signal frequency resolution, OBO operation point, and PAE at the same operation point.

By adhering to these specifications enables more accurate and meaningful comparison of NPR performance across different studies and applications, facilitating the development of reliable and efficient designs in the field of SatCom.

V. Conclusion

This paper has presented the design strategy and extensive linearity characterization of a GaN-Si MMIC Doherty power amplifier for Ka-band satellite downlink. The target application is one where additional linearization is impractical and often unfeasible, hence the need of optimizing the intrinsic linearity of the DPA and minimizing the use of linearizers. Despite the target linearity is expressed in terms of NPR, the DPA design relies on single- and two-tone metrics, namely AM/PM and IMR. This work has highlighted the differences between two-tone and system level linearity metrics yet demonstrating that a successful design can be achieved with the adopted strategy. In fact, the DPA achieves state-of-the-art performance both in terms of efficiency and linearity, also under very wideband (2.9 GHz instantaneous bandwidth) modulated signal excitation. The paper has also explored the impact of signal statistics and nonlinear dynamic effects on the NPR and provided guidelines for unambiguous specification of the desired NPR target.

Acknowledgments

This research was carried out under a programme of and funded by the European Space Agency (contract "Single-chip Ka-band Doherty amplifier" ITT: AO/1-9088/17/NL/HK Ref:Item no. 17.1ET.01). The view expressed herein can in no way be taken to reflect the official opinion of the ESA.

This research was also partially supported by the Project Programma Operativo Nazionale (PON) Ricerca e Innovazione "Tecnologie abilitanti e architetture innovative per future generazioni (6G) di trasmettitori intelligenti green" (DM 1062/21, CUP E15F21003760001) funded by the Italian Ministry of University and Research (MUR).

The authors would like to acknowledge Dr. Václav Valenta for the fruitful discussions.

References

[1] A. Rofougaran, M. Rofougaran, and A. Behzad, "Radios for next-generation wireless networks," *IEEE Microw. Mag.*, vol. 6, no. 1, pp. 38–43, 2005.

[2] H. Yang, T. Jiang, L. Yang, and J. Shi, "Performance analysis of OFDM systems with high peak-to-average power ratios: A large deviations approach," *IEEE Trans. Wireless Commun.*, vol. 11, no. 11, pp. 4003–4013, Nov. 2012.

[3] A. Jacomb-Hood and E. Lier, "Multibeam active phased arrays for communications satellites," *IEEE Microw. Mag.*, vol. 1, no. 4, pp. 40–47, 2000.

[4] M. Hangai, T. Torii, Y. Yamaguchi, K. Nakatani, S. Shinjo, and K. Yamanaka, "Microwave and Millimeter-Wave GaN Amplifiers for Satellite Communications," in *2018 Asia-Pacific Microwave Conference (APMC)*, 2018, pp. 70–72.

[5] R. Giofrè, A. Piacibello, P. Colantonio, and V. Camarchia, "Gallium Nitride Power Amplifiers for Ka-Band Satcom Applications: Requirements, Trends, and the Way Forward," *IEEE Microw. Mag.*, vol. 24, no. 12, pp. 74–86, 2023.

[6] W. Doherty, "A New High Efficiency Power Amplifier for Modulated Waves," *Proceedings of the Institute of Radio Engineers*, vol. 24, no. 9, pp. 1163–1182, 1936.

[7] J. C. Pedro, M. Ferreira, and L. M. Pessoa, "Doherty power amplifiers: From the basics to next-generation architectures," *IEEE Trans. Microw. Theory Techn.*, vol. 62, no. 6, pp. 1664–1678, Jun. 2014.

[8] E. Richard, T. Huet, H. M. Karimdjy, M. Camiade, C. Chang, V. Serru, F. Fernandez, J. Suedois, I. Davies, and V. Valenta, "A 17.3-20.3 GHz Doherty Power Amplifier with 14 W Saturated Output Power and 28% PAE at 6 dB OPBO in 150 nm GaN Technology," in *2022 IEEE/MTT-S International Microwave Symposium - IMS 2022*, 2022, pp. 422–425.

[9] A. Piacibello, R. Giofrè, R. Quaglia, R. Figueiredo, N. Carvalho, P. Colantonio, V. Valenta, and V. Camarchia, "A 5-W GaN Doherty Amplifier for Ka-Band Satellite Downlink With 4-GHz Bandwidth and 17-dB NPR," *IEEE Microw. Wireless Compon. Lett.*, vol. 32, no. 8, pp. 964–967, 2022.

[10] C. Boulanger, A. Mallet, J. Puech, L. Lapierre, and J. Sombrin, "A new criterion for power amplifier comparison and optimisation," in *IEE Seminar on Microwave and RF Power Amplifiers (Ref. No. 2000/118)*, 2000, pp. 1/1–1/6.

[11] R. Figueiredo, N. B. Carvalho, A. Piacibello, and V. Camarchia, "Nonlinear Dynamic RF System Characterization: Envelope Intermodulation Distortion Profiles–A Noise Power Ratio-Based Approach," *IEEE Trans. Microw. Theory Techn.*, vol. 69, no. 9, pp. 4256–4271, 2021.

[12] S. Din, A. M. Morishita, N. Yamamoto, C. Brown, M. Wojtowicz, and M. Siddiqui, "High-power K-band GaN PA MMICs and module for NPR and PAE," in *2017 IEEE MTT-S International Microwave Symposium (IMS)*, 2017, pp. 1838–1841.

[13] V. Valenta, I. Davies, N. Ayllon, S. Seyfarth, and P. Angeletti, "High-gain GaN Doherty power amplifier for Ka-band satellite communications," in *2018 IEEE Topical Conference on RF/Microwave Power Amplifiers for Radio and Wireless Applications (PAWR)*, 2018, pp. 29–31.

[14] T. Torii, M. Hangai, R. Inagaki, and S. Shinjo, "High Efficient Design of K-Band GaN Power Amplifier with bias optimization for high linearity," in *2019 IEEE Asia-Pacific Microwave Conference (APMC)*, 2019, pp. 473–475.

[15] C. Nogales, Z. Popović, and G. Lasser, "A 10-W6-12GHz GaN MMIC Supply Modulated Power Amplifier," in *2022 52nd European Microwave Conference (EuMC)*, 2022, pp. 436–439.

[16] R. Figueiredo and N. Carvalho, "Linearity Metrics and Signal Statistics - The Need for Standards," in *2022 IEEE/MTT-S International Microwave Symposium - IMS 2022*, 2022, pp. 868–871.

[17] N. Borges de Carvalho and J. Pedro, "A comprehensive explanation of distortion sideband asymmetries," *IEEE Trans. Microw. Theory Techn.*, vol. 50, no. 9, pp. 2090–2101, 2002.

[18] L. Piazzon, R. Giofrè, R. Quaglia, V. Camarchia, M. Pirola, P. Colantonio, F. Giannini, and G. Ghione, "Effect of Load Modulation on Phase Distortion in Doherty Power Amplifiers," *IEEE Microw. Wireless Compon. Lett.*, vol. 24, no. 7, pp. 505–507, 2014.

[19] L. C. Nunes, P. M. Cabral, and J. C. Pedro, "AM/PM distortion in GaN Doherty power amplifiers," in *2014 IEEE MTT-S International Microwave Symposium (IMS2014)*, 2014, pp. 1–4.

[20] V. Camarchia, P. Colantonio, F. Giannini, R. Giofrè, T. Jiang, M. Pirola, R. Quaglia, and C. Ramella, "A Design Strategy for AM/PM Compensation in GaN Doherty Power Amplifiers," *IEEE Access*, vol. 5, pp. 22 244–22 251, 2017.

[21] X. Fang, A. Chung, and S. Boumaiza, "Linearity-Enhanced Doherty Power Amplifier Using Output Combining Network With Predefined AM–PM Characteristics," *IEEE Trans. Microw. Theory Techn.*, vol. 67, no. 1, pp. 195–204, 2019.

[22] G. Gonzalez, "Microwave Transistor Amplifiers: Analysis and Design," 1997.

[23] I. Dettmann, L. Wu, and M. Berroth, "Comparison of a single-ended class AB, a balance and a Doherty power amplifier," in *2005 Asia-Pacific Microwave Conference Proceedings*, vol. 2, 2005, pp. 4 pp.–.

[24] A. Piacibello, R. Quaglia, R. Giofrè, R. Figueiredo, P. Colantonio, N. B. Carvalho, V. Valenta, and V. Camarchia, "High-Gain and High-Linearity MMIC GaN Doherty Power Amplifier With 3-GHz Bandwidth for Ka-Band Satellite Communications," *IEEE Microw. Wireless Techn. Lett.*, vol. 34, no. 6, pp. 765–768, 2024.

[25] A. Piacibello, P. Colantonio, R. Giofrè, and V. Camarchia, "Doherty Power Amplifiers for Ka-Band Satellite Downlink," in *2022 IEEE Topical Conference on RF/Microwave Power Amplifiers for Radio and Wireless Applications (PAWR)*, 2022, pp. 18–21.

[26] R. Quaglia, A. Piacibello, F. Costanzo, R. Giofrè, M. Casbon, R. Leblanc, V. Valenta, and V. Camarchia, "Source/Load-Pull Characterisation of GaN on Si HEMTs with Data Analysis Targeting Doherty Design," in *2020 IEEE Topical Conference on RF/Microwave Power Amplifiers for Radio and Wireless Applications (PAWR)*, 2020, pp. 5–8.

[27] N. Carvalho and J. Pedro, "Two-tone IMD asymmetry in microwave power amplifiers," in *2000 IEEE MTT-S International Microwave Symposium Digest (Cat. No.00CH37017)*, vol. 1, 2000, pp. 445–448 vol.1.

[28] D. R. Barros, L. C. Nunes, P. M. Cabral, and J. C. Pedro, "Impact of the Input Baseband Terminations on the Efficiency of Wideband Power Amplifiers Under Concurrent Band Operation," *IEEE Trans. Microw. Theory Techn.*, vol. 67, no. 12, pp. 5127–5138, 2019.

[29] J. Brinkhoff and A. Parker, "Effect of baseband impedance on FET intermodulation," *IEEE Trans. Microw. Theory Techn.*, vol. 51, no. 3, pp. 1045–1051, 2003.

[30] M. Akmal, J. Lees, S. Bensmida, S. Woodington, V. Carrubba, S. Cripps, J. Benedikt, K. Morris, M. Beach, J. McGeehan, and P. J. Tasker, "The effect of baseband impedance termination on the linearity of GaN HEMTs," in *The 40th European Microwave Conference*, 2010, pp. 1046–1049.

[31] L. C. Nunes, D. R. Barros, P. M. Cabral, and J. C. Pedro, "Efficiency Degradation Analysis in Wideband Power Amplifiers," *IEEE Trans. Microw. Theory Techn.*, vol. 66, no. 12, pp. 5640–5651, 2018.

[32] F. Costanzo, V. Camarchia, N. B. Carvalho, P. Colantonio, A. Piacibello, R. Quaglia, V. Valenta, and R. Giofrè, "A GaN MMIC Stacked Doherty Power Amplifier For Space Applications," in *2022 IEEE Topical Conference on RF/Microwave Power Amplifiers for Radio and Wireless Applications (PAWR)*, 2022, pp. 29–31.

[33] M. Cullen, M. Cavin, L. Hoover, and A. Cherrette, "Noise Power Ratio Prediction and Measurement of a Ku band GaN Power Amplifier," in *2019 93rd ARFTG Microwave Measurement Conference (ARFTG)*, 2019, pp. 1–4.

[34] R. Figueiredo, S. Chaudhary, M. V. Bossche, M. Rousstia, M. Marchetti, and N. B. Carvalho, "Discussion on system-level wideband active load-pull linearity measurements: How to reach broadband design techniques?" in *2024 102nd ARFTG Microwave Measurement Conference (ARFTG)*, 2024, pp. 1–3.

[35] T. Reveyrand, D. Barataud, J. Lajoinie, M. Campovecchio, J.-M. Nebus, E. Ngoya, J. Sombrin, and D. Roques, "A Novel Experimental Noise Power Ratio Characterization Method for Multicarrier Microwave Power Amplifiers," in *55th ARFTG Conference Digest*, vol. 37, 2000, pp. 1–5.

[36] N. B. Carvalho, K. A. Remley, D. Schreurs, and K. G. Gard, "Multisine signals for wireless system test and design [Application Notes]," *IEEE Trans. Multimedia*, vol. 9, no. 3, pp. 122–138, 2008.

[37] R. W. Koch, "Random Signal Method of Nonlinear Amplitude Distortion Measurement," *IEEE Trans. Instrum. Meas.*, vol. IM-20, no. 2, pp. 95–99, 1971.

[38] N. De Carvalho and J. Pedro, "Large- and small-signal IMD behavior of microwave power amplifiers," *IEEE Trans. Microw. Theory Techn.*, vol. 47, no. 12, pp. 2364–2374, 1999.

[39] J. Pedro and N. De Carvalho, "On the use of multitone techniques for assessing RF components' intermodulation distortion," *IEEE Trans. Microw. Theory Techn.*, vol. 47, no. 12, pp. 2393–2402, 1999.

[40] R. Figueiredo and N. Carvalho, "Two-Tone Signals Harmonic Conditions for PAPR Variation," in *2022 International Workshop on Integrated Nonlinear Microwave and Millimetre-Wave Circuits (INMMiC)*, 2022, pp. 1–3.